Article

Symmetric and Asymmetric Semi-Metallic Gasket Cores and Their Effect on the Tightness Level of the Bolted Flange Joint

Przemysław Jaszak [1],* and Rafał Grzejda [2],*

[1] Faculty of Mechanical and Power Engineering, Wroclaw University of Science Technology, Wybrzeze Stanislawa Wyspianskiego St. 27, 50-370 Wroclaw, Poland

[2] Faculty of Mechanical Engineering and Mechatronics, West Pomeranian University of Technology in Szczecin, 19 Piastow Ave., 70-310 Szczecin, Poland

* Correspondence: przemyslaw.jaszak@pwr.edu.pl (P.J.); rafal.grzejda@zut.edu.pl (R.G.)

Abstract: The paper presents the effect of the symmetric and asymmetric semi-metallic gasket core shape on the tightness level in bolted flange joints. Experimental tests, as well as numerical calculations based on the finite element method, revealed that the asymmetric gasket core provides a higher strain on the sealing graphite layer and leads to a more uniform distribution of strain on the particular ridges of the core. Furthermore, the leakage rate of the asymmetric gasket was reduced by approximately 60% compared to the symmetric gasket. It was also observed that the uniformity of pressure and strain distribution in a gasket with an asymmetric core occurs over about 80% of the gasket width. The leakage reduction effect in a flange joint sealed with a gasket with an asymmetric core was theoretically explained. As shown, the main leakage flows through the porous structure of the graphite layer, while the leakage path at the interface between the metal rough profile and the graphite layer is several orders of magnitude smaller.

Keywords: semi-metallic gasket; tightness level; bolted flange joint

1. Introduction

Bolted joints are one of the most commonly used solutions for connecting flanges in piping systems [1–4]. Both symmetric and asymmetric fastener arrangements are used in these joints. The asymmetric geometry combined with the asymmetric fastener arrangement usually results in an uneven loading condition of the joint.

Non-uniformity in loading on parts of machines and equipment is an undesirable phenomenon, influencing reduced durability or unexpected destruction. One of the main design problems in this case is to minimise, and equalise, the load in the form of forces, moments and their derivatives, i.e., stresses [5–7]. An asymmetric load condition significantly reduces the fatigue life of machine parts, as exemplified by the results of numerous papers on the subject [8,9]. The levelling or reduction in the stress distribution can be realised via the so-called flexibility of the structure in regions of high stress concentration.

A typical device that is subjected to an uneven load condition is a bolted flange joint with a gasket [10–12]. As it turns out, all its components are subjected to uneven loading [13]. Flanges are subjected to bending as a result of bolt tension [14]. The deformation of the flange due to bending induces the bending of the bolt and also causes uneven pressure distribution on the contact surface of the gasket [15]. The effects of excessive flange deformation on the load condition of the joint and the level of gasket leakage are presented in [16,17]. Exceeding the permissible contact stress of a gasket can lead, for example, to the buckling of the inner coils—as occurs in a spiral gasket [18–20]. There are many examples of

papers describing experimental tests [21–25] or numerical tests [26–30] of gasketed bolted flange joints. A review of these provides an insight into the phenomena occurring during non-uniform loading of these joints.

One way to equalise the pressure distribution on the gasket surface is to choose the right elasticity. The most commonly used type of gaskets, which have developed quite strongly in recent times, is semi-metallic gaskets [31]. They constitute a group of so-called high-performance gaskets, used at high pressure and temperature. Their characteristic feature is a construction consisting partly of metal and the remaining part of a soft material, the so-called filler [32,33]. The metal part can be the internal reinforcement of the gasket, e.g., in the form of a metal mesh, tape or sheet covered with a filler material. In other solutions, the metal part may be on the outer surface of the soft material, e.g., by fitting it completely. In the latter case, the soft material gives the gasket more flexibility while the metal part performs the sealing function. One of the most common solutions for a semi-metallic gasket is the multi-edge gasket. Its construction consists of a metal core (usually made of acid-resistant steel), whose serrated faces are covered with a filling material [34,35]. The filling material can be expanded graphite [36]. The advantages of this solution were presented in [34], analysing the effect of the shape of the gasket core on the level of leakage. As it turns out, making the core more flexible by undercutting its edges has a significant impact on the distribution of contact pressure that prevails at the faces.

The aim of the present study, in contrast to the results presented in [34,35], is to estimate the leakage at relatively low contact pressure. According to research [35], the strain of the graphite layer above a certain value fixes its permeability at a constant level. Below this value, the permeability is strongly dependent on the local strain value of the sealing layer. In the present study, an attempt was made to determine, analytically and numerically, the leakage at a non-uniform pressure distribution of the sealing graphite layer, for which the permeability depends on the local strain value. A model of fluid flow through a ring-shaped porous bed was adapted for this purpose.

On the basis of the tests carried out, it was shown that the asymmetric gasket core provides greater strain on the sealing graphite layer and leads to a more uniform distribution of strain on the individual ridges of the core. In addition, the leakage reduction effect in a flange joint sealed with a gasket with an asymmetric core was theoretically explained. It was also shown that the main leakage flows through the porous structure of the graphite layer, while the leakage path at the interface between the metal rough profile and the graphite layer is several orders of magnitude smaller.

2. Materials and Methods

2.1. Research Object

The object of the research was a multi-edge gasket made in two variants that differed in the shape of the cross-section of the metal core. The first variant had a core with a standard symmetric (rectangular) shape, while the second variant was characterised by an asymmetric cross-sectional shape that had a circumferential notch on the outer diameter of the core. Both variants are shown in Figure 1.

The advantages of a gasket solution with an undercut core were presented, among others, in [34], in which it was shown that such a solution significantly improves the tightness of the bolted flange joint.

The metal core was made from 316L steel, while the caps were made from expanded graphite with a thickness of 1 mm and a density of 1 g/cm^3. The main overall dimensions of both structures (inner and outer diameter and thickness, as well as the shape and number of core edges cut into the faces) followed directly from EN 1514-6 [37,38].
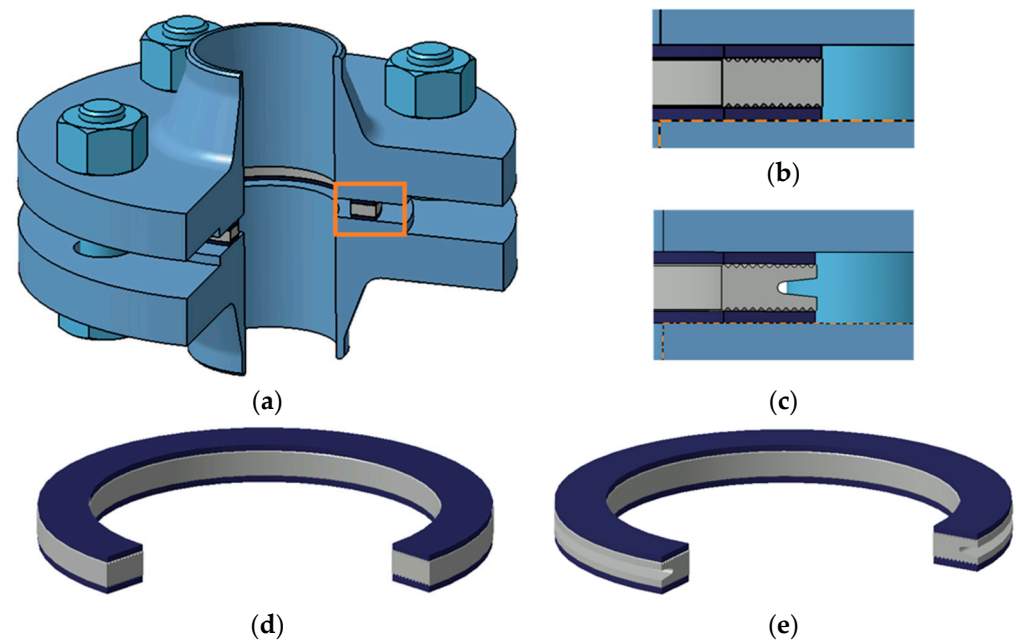
Figure 1. Components of the bolted flange joint: (**a**) view of the joint; (**b**) gasket section with symmetric core; (**c**) gasket section with asymmetric core; (**d**) view of the gasket with symmetric core; (**e**) view of the gasket with asymmetric core.

2.2. Numerical Calculations

The objective of the numerical calculations was to determine the pressure and strain distributions on the surface of the graphite sealing layer, which deforms unevenly when in contact with the multi-edged surface of the metal core. The results of the calculations, mainly in the form of averaged strain values of the graphite layer on the individual ridges of the metal core, provided the necessary data for estimating the leakage value in an analytical manner. The calculations were performed in Ansys Workbench 19.1 (Ansys, Inc., Southpointe 2600 Ansys Drive, Cecil Township, PA 15317, USA) using structural static analysis [39,40].

2.2.1. Calculation Model

The computational model was a fragment of a DN40 PN40 bolted flange joint [41,42] with a multicore gasket in two configurations, i.e., with the symmetric and asymmetric core. In order to speed up the calculations, the geometric model was simplified to a joint fragment reflecting its cyclicity with respect to the axis of rotation and using symmetry in the horizontal split plane of the gasket [43–46]. The adopted model in the form of a three-dimensional joint slice with an angle of 1° is shown in Figure 2. This calculation approach is fully acceptable and approved by the Pressure Vessel Research Council (PVRC), as presented in [47]. The model in this form has no bolt geometry the same approach used in [48]. The load on the joint and the gasket, resulting from bolt tension, is in this case induced via the displacement applied at the point of contact between the bolt head (or nut) and the flange. The target value of bolt tension is measured using the reaction force induced via the displacement of the flange on the restrained part of the gasket core.

SOLID186 higher-order shape function elements [49,50] were used to discretise the model. The finite element mesh is shown in Figure 3. The basic finite element size in the flange geometry area was 2 mm. For the metal core and graphite overlays, the element edge size was 0.01 mm and 0.05 mm, respectively.
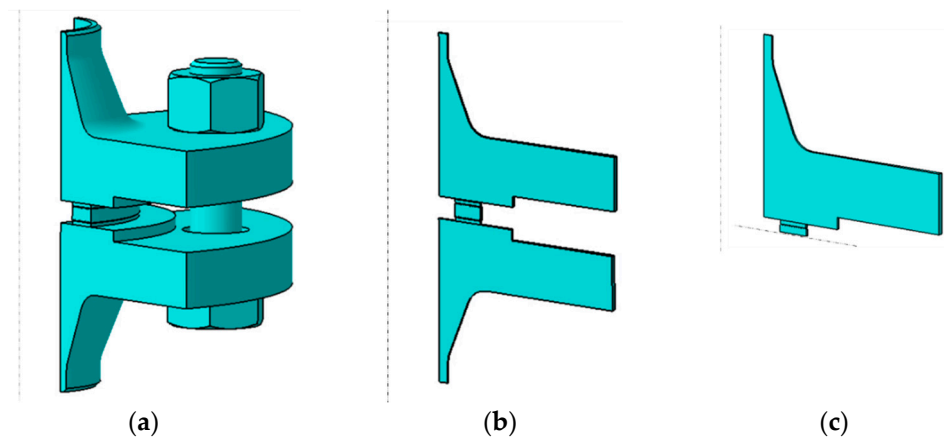
Figure 2. Model of the joint: (**a**) geometry simplified to 1/4 of the actual model; (**b**) geometry simplified to 1/360 of the actual model; (**c**) geometry simplified to 1/360 of the actual model and using symmetry in the gasket centre plane.
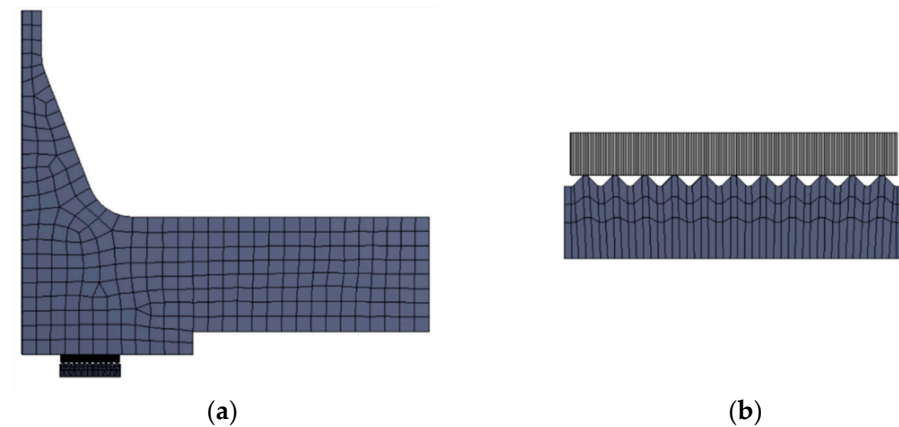

Figure 3. Discrete model of the joint: (**a**) view of the full finite element mesh; (**b**) finite element mesh in the vicinity of the gasket core and sealing layer.

To investigate the effect of the grid size used to discretise the graphite layer on its strain values, a mesh-independent test was performed. The results of these calculations are shown in Figures 4 and 5.

An elastic model was used to represent the mechanical properties of the flange and the gasket core, assuming a value of Young's modulus and Poisson's ratio. The material properties of the metal part of the joint were collected in Table 1. To represent the properties of the graphite caps, a non-linear gasket-type model available in the material database of the calculation programme used was applied. The compression characteristics of the graphite introduced in this material model were obtained from tests (based on EN 13555 [51,52]). The course of this characteristic is shown in Figure 6.
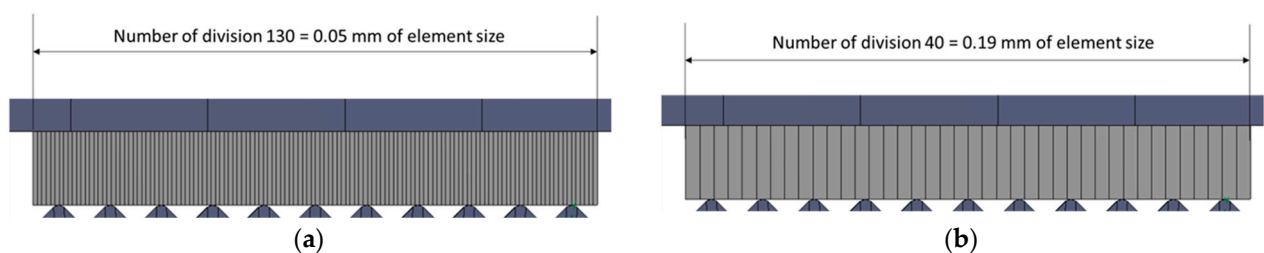

Figure 4. Mesh-independent test of the graphite layer: (**a**) mesh view with an element size of 0.05 mm; (**b**) mesh view with an element size of 0.19 mm.
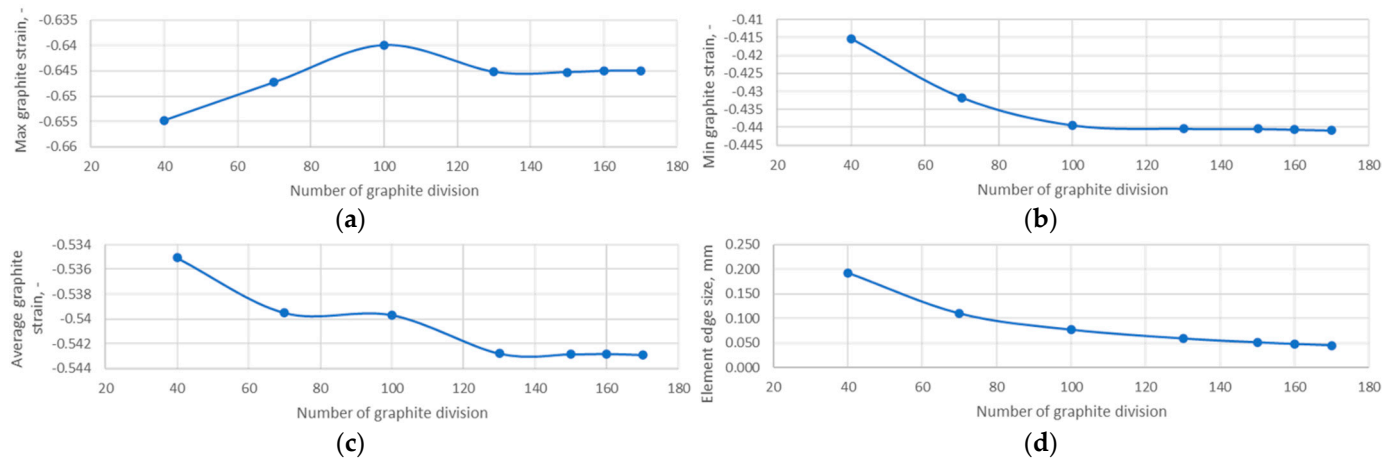
Figure 5. Results of the mesh-independent test of the graphite layer: (**a**) maximum graphite strain; (**b**) minimum graphite strain; (**c**) average graphite strain; (**d**) element edge size.

Table 1. Material properties of the metal parts of the joint.

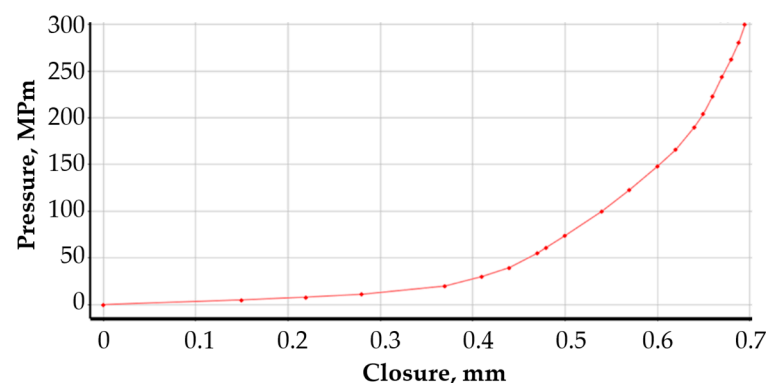| Part	Material	Young's Modulus, GPa	Compression Strength, MPa	Poisson's Ratio, –
Flange	304L (1.4307)	197	115	0.3
Gasket core	316L (1.4404)	200	220	0.3

Figure 6. Compressive characteristics of a 1 mm-thick graphite sealing layer.

2.2.2. Boundary Conditions

The model was restrained in the horizontal plane of symmetry of the core division. A rotation constraint about the axis and a displacement constraint in the radial direction were applied to the cylindrical part of the flange neck. At the point of contact between the bolt head and the flange, a displacement was introduced to simulate its deformation resulting from the gradual tightening of the nut. This simulated the tension of the bolt. The specific values of the flange displacement applied at the bolt location were determined by measuring the reaction forces on the fixed support of the model. The total reaction force is the sum of the four bolt tensions. The relationship between the bolt force (as one-quarter of the reaction force) and flange displacement (in the bolt area) is shown in Figure 7.

A pressure of 4 MPa was applied to the inner walls of the model from the pressure of the medium to be sealed. The maximum displacement value was 0.8 mm. The target tension for a single bolt was 25 kN. The boundary conditions are presented in Figure 8. The contact between the graphite surface and the metal surfaces of the flange and the sealing core was defined as frictional, with the graphite surface set as 'Contact' and the metal surfaces as 'Target'. The discretisation parameters of the contact surfaces are presented in Table 2.
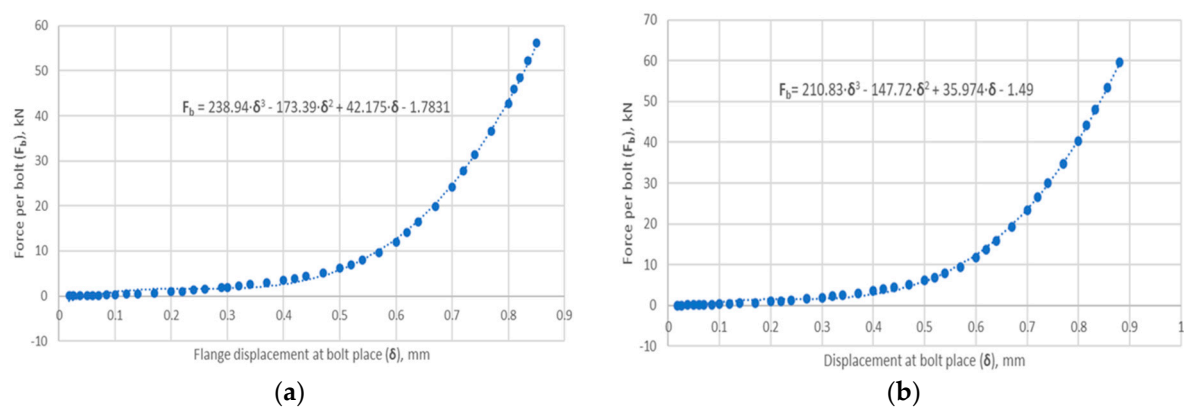
(**a**)

(**b**)

Figure 7. The relationship between the bolt force (as one-quarter of the reaction force) and flange displacement for (**a**) joint with symmetric gasket and (**b**) joint with asymmetric gasket.
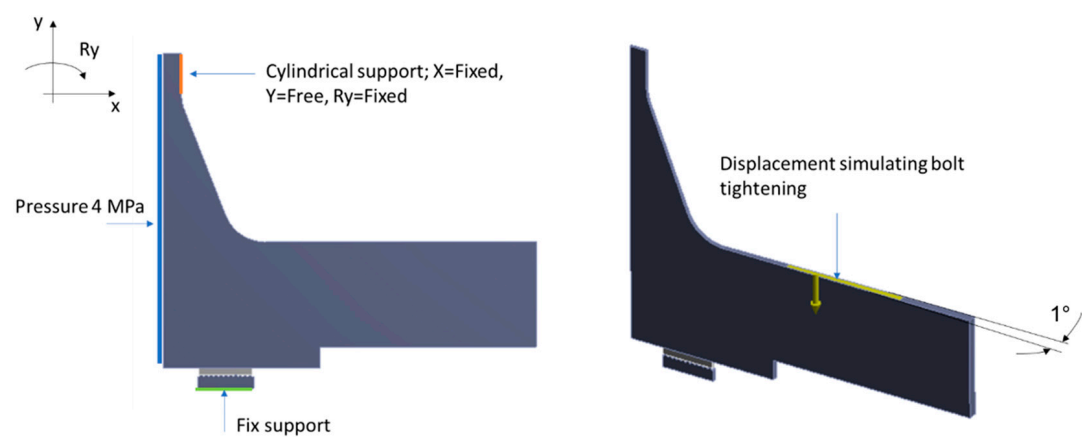

Figure 8. Boundary conditions of the calculation model.

Table 2. Contact conditions at the graphite-metal interface.

Type of Contact	Frictional
Friction value	From 0.1 to 0.3 with an increment of 0.05
Contact behaviour	Symmetric
Formulation	Augmented Lagrange
Detection method	On Gauss point
Penetration tolerance	0.01 mm
Normal stiffness factor	1

2.3. Analytical Calculations

The objective of the analytical calculations was to estimate the leakage through the graphite caps of the analysed sealing solutions in two variants of the shape of the metal core. A model of fluid flow through a cylindrical porous bed, shown in Figure 9, was adopted as the analytical model.
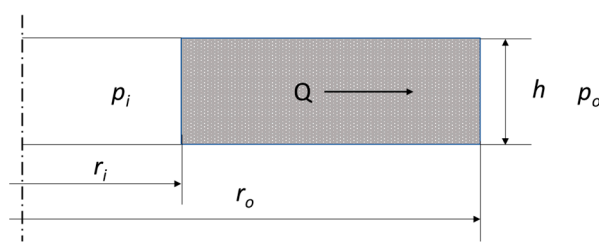

Figure 9. Geometric model of fluid flow through a porous bed in the form of a cylinder.

The equation linking the basic geometrical data of the porous bed, and the properties of the medium are described in the following equation:

$$Q = \frac{2\pi h K_V (p_o - p_i)}{\mu \ln\left(\frac{r_o}{r_i}\right)} \tag{1}$$

where h denotes the bed thickness, K_V denotes the bed permeability, p_i and p_o denote the pressure inside and outside of the cylinder, respectively, μ denotes the dynamic fluid viscosity, and r_i and r_o denote the inner and outer radius of the cylinder.

Equation (1) allows the flow through a porous gasket layer to be modelled when the contact pressure on the gasket surface is uniform. Otherwise, the thickness of the layer (cap) and its permeability depends on its degree of deformation (compression). When the contact pressure on the sealing surface is uneven, it seems appropriate to isolate the zones (sealing widths) in which there is quasi-uniform pressure, calculate the permeability and layer thickness in these zones, and then add up the resulting partial values. In the case of the structure shown in Figure 1, the pressure concentration zones of the graphite layer are caused by the individual ridges cut into the metal core of the gasket. By transforming Equation (1), it is possible to count the pressure drop that will occur as a result of fluid flow through a single zone of pressure concentration of the graphite layer, caused by a given ridge of the gasket with known inner and outer radii, r_i and r_{i+1}:

$$\Delta p = \frac{Q \mu \ln\left(\frac{r_{i+1}}{r_i}\right)}{2\pi h K_V} \tag{2}$$

The total pressure drop across the individual pressure-back zones, Δp, must be equal to the total pressure drop that occurs between the inner and outer surfaces of the graphite layer:

$$\Delta p = \Delta p_i + \Delta p_{i+1} + \cdots + \Delta p_n \tag{3}$$

where Δp_i denotes the pressure drop of the fluid in the i-th zone of contact pressure concentration of the graphite layer, Δp_{i+1} denotes the pressure drop of the fluid in the next adjacent zone of pressure concentration of the graphite layer, and Δp_n denotes the pressure drop of the fluid in the n-th (last) zone of contact pressure concentration of the graphite layer.

As the fluid flow through the layer is constant, the pressure difference across the outer and inner diameters is known, so the fluid flow through the layer with uneven contact pressure distribution can be calculated from the following equation:

$$Q = \frac{2\pi (p_o - p_i)}{\mu} \cdot \sum_{i=1}^{n} \left(\frac{h_i K_{Vi}}{\ln\left(\frac{r_{i+1}}{r_i}\right)} \right) \tag{4}$$

In addition, it can be assumed that at each of the ridges of the metal core, the strain and pressure of the graphite sealing layer were brought to an average value. A graphical interpretation of Equation (4) is shown in Figure 10.

As the thickness of the graphite layer in each zone is strain-dependent, the following can be written:

$$h = h_0 (1 - \varepsilon) \tag{5}$$

where h_0 denotes the nominal thickness of the graphite layer, and ε denotes the strain of the graphite layer.
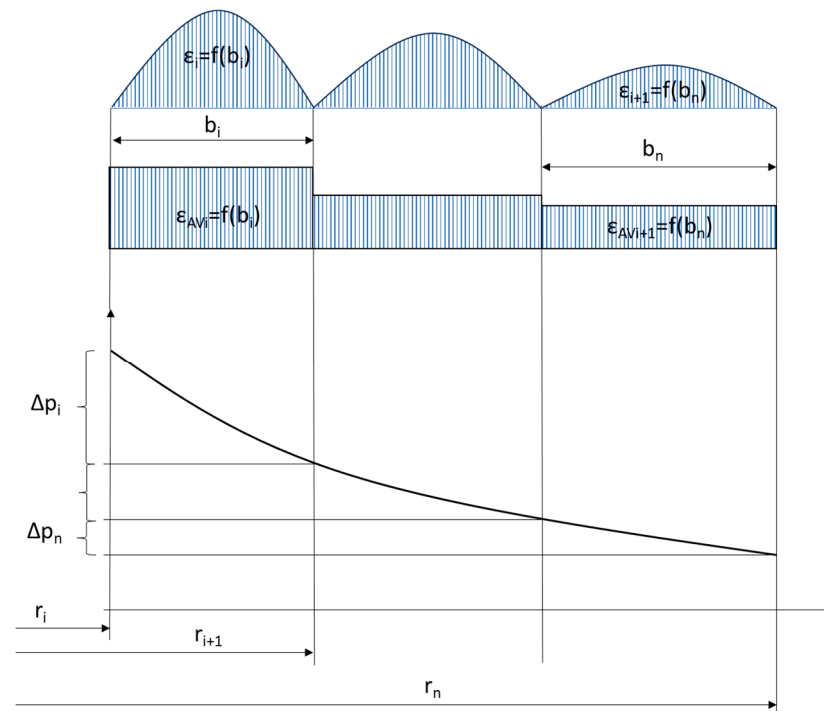
Figure 10. Graphical interpretation of the calculation of the partial strain and permeability values of the graphite sealing layer in the different concentration zones.

Furthermore, when the fact that there are two graphite layers in the gasket is taken into account, the density of the fluid is known, and the leakage is related to the average circumference of the gasket, conclusively, Equation (4) can be written in the following form:

$$Q = \frac{2h_0(p_o - p_i)\rho}{\mu r_{AV}} \cdot \sum_{i=1}^{n} \left(\frac{(1 - \varepsilon_i)K_{Vi}}{\ln\left(\frac{r_{i+1}}{r_i}\right)} \right) \tag{6}$$

where ρ denotes the density of the fluid to be sealed, ε_i denotes the strain of the *i*-th zone of the graphite layer, and r_{AV} denotes the average gasket radius.

2.4. Experimental Research

Figure 11 shows the test rig. It consists of two blinded flanges with dimensions corresponding to the DN40 PN40 designation, four M16 bolt connections, micrometres (to measure bolt deformation during tensioning), a helium detector, and a bottle of helium.

The measurement of bolt elongation was based on the method given in DIN 28090-3 [53,54]. It consists of measuring the distance between the face of the bolt shank and the face of the rod embedded in the bolt. Based on the previously determined stiffness characteristics of each bolt (in a tensile test on a testing machine), the relationship between the tension force of the bolt and its elongation was known. Two edge gasket solutions, geometrically identical to the models shown in Figure 1, were used in the tests.

The objective of the research was to determine the leakage as a function of the tension force of a single bolt. Bolt tension was induced with a torque spanner by tracking the elongation of a given bolt on a micrometre sensor. Bolt tension values ranged from 5 kN to 25 kN with increments of 5 kN. Once the appropriate bolt tension was induced, the joint was sealed in a glass dome. Subsequently, a pressure value of 4 MPa was set on the helium bottle pressure-reducing valve and the medium was introduced inside the bolted flange joint. At each set bolt tension value, the tightness of the joint was measured using a spectrometric leak detector [55].
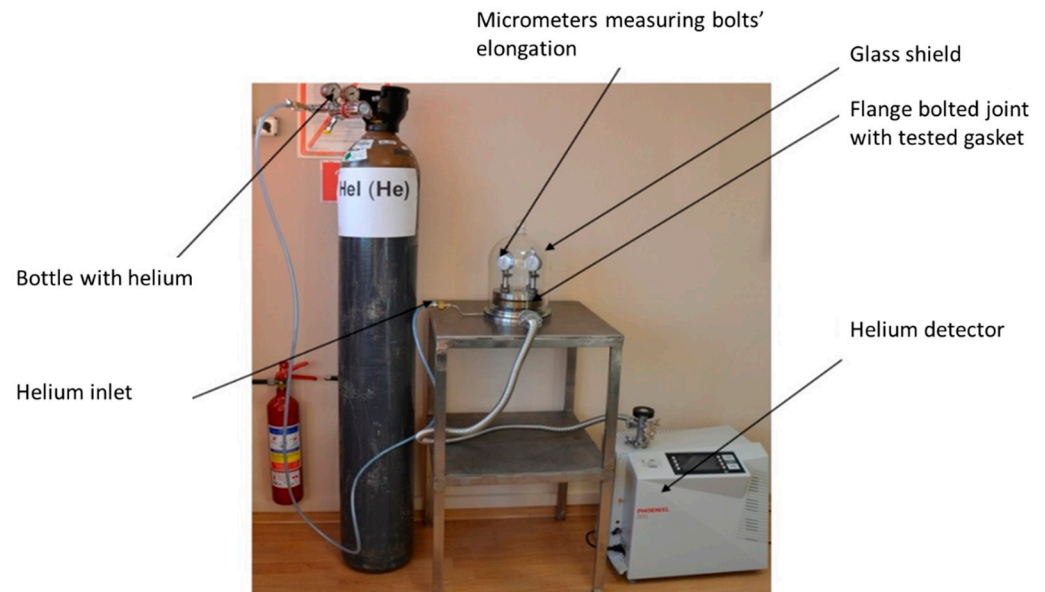
Figure 11. Test stand used in experimental research.

3. Results

3.1. Results of Numerical Calculations

Figure 12 shows the distribution of contact pressure and strain between the graphite sealing layer at the particular ridges of the metal core of the gasket.
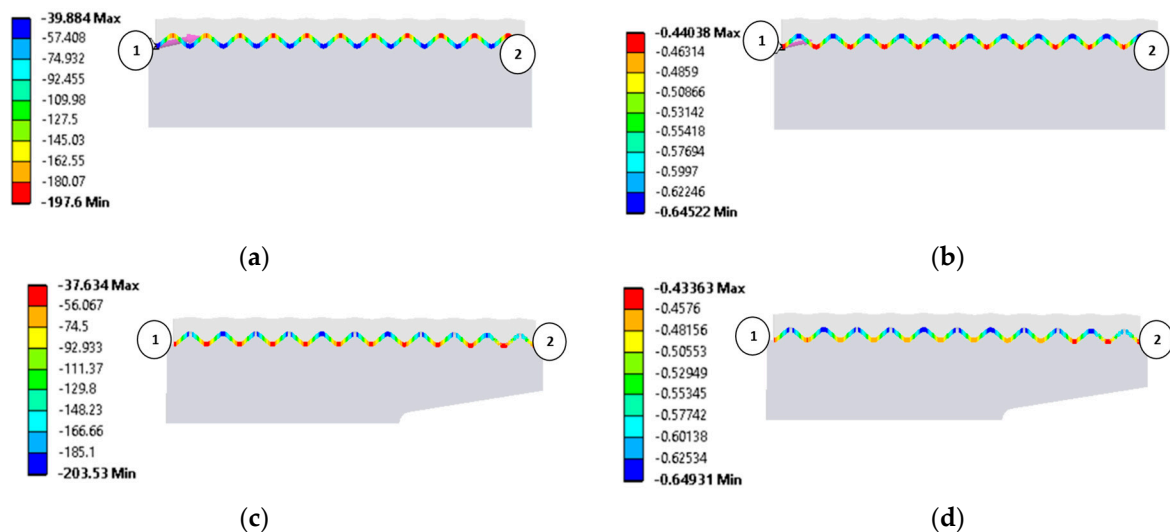

(**a**)

(**b**)

(**c**)

(**d**)

Figure 12. Results of numerical calculations: (**a**) contact pressure between the graphite layer and the ridges of the symmetric gasket core (MPa); (**b**) strain of graphite layer for the symmetric gasket core (mm); (**c**) contact pressure between the graphite layer and the ridges of the asymmetric gasket core (MPa); (**d**) strain of graphite layer for the asymmetric gasket core (mm).

The pressure was measured along a measurement path defined in the direction from the inner diameter of the gasket (marked in Figure 12a,b by point 1) to the outer diameter of the gasket (marked in Figure 12a,b by point 2). Figure 12a,b show the pressure and strain distributions in the gasket with the symmetric core, while Figure 12c,d show the pressure and strain distributions in the gasket with the asymmetric core.

To better illustrate the effect of the core shape on the graphite layer strain, its progression is shown in the form of graphs in Figure 13. It can be seen that the symmetric core induces a gradual increase in the graphite layer strain as the outer diameter of the gasket is

approached. In the case of the gasket with the asymmetric core shape, the highest layer strain has moved to the inner diameter region and maintains an almost constant value up to about 80% of the gasket width. The decrease in strain of the graphite layer drops only at the last three ridges of the core.
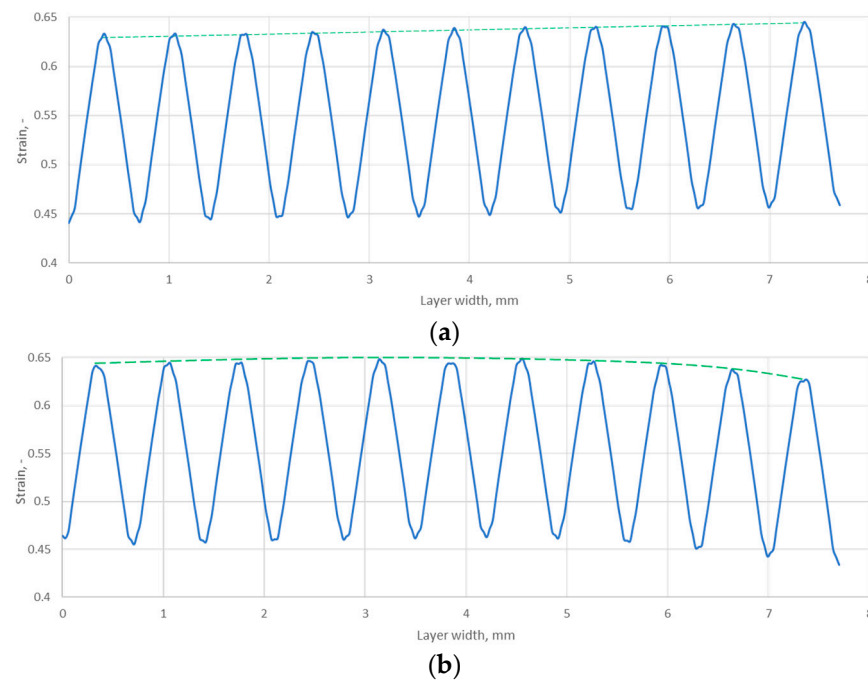
(**a**)

(**b**)

Figure 13. Strain distribution of the graphite layer along the width of the gasket for (**a**) symmetric core and (**b**) asymmetric core.

3.2. Results of Analytical Calculations

Table 3 presents a summary of the results of the analytical calculations in the form of the average strain of the graphite layer, the permeability, and the radii characterising the position of a given ridge pile-up zone (determined by the inner and outer diameters of a given ridge cut on the core). It should be noted that the average strain values of the graphite layer were calculated from the results of the numerical calculations as the arithmetic mean value from the pile-up at each ridge (for the data in Figure 13). In turn, the permeability value in each zone was counted as a function of the arithmetic mean strain of the zone. The dependence of the permeability relationship as a function of strain is shown in Figure 14. The fit of the regression curve to the obtained characteristic points was reached with a determination coefficient R^2 of 0.998. The effect of the uniformity of the strain of the graphite layer, and the transfer of its maximum value to the inner diameter area of the gasket, is very beneficial. As shown in [34], the concentration of contact pressure and sealing layer strain is closer to the inner diameter, the sealing tightness increases.

The equation describing permeability as a function of strain was defined as follows:

$$K_V = 2\varepsilon^{-12.98} \times 10^{-18} \tag{7}$$

Based on Equations (6) and (7), the fluid leakage through the graphite sealing layer was calculated at the maximum applied tension of a single bolt of 25 kN. The calculated leakage values are shown in Figure 15. For the gasket with the symmetrical core, the leakage is almost three times higher. The analytically calculated leakage was 3.57×10^{-3} mg/(s·m) and 1.21×10^{-3} mg/(s·m) for the symmetrical and asymmetrical core cases, respectively.

Table 3. Partial strain and permeability values at individual ridges of the gasket core.

Parameters	Core ridge No. 1 Symmetric core	Asymmetric core	Parameters	Core ridge No. 2 Symmetric core	Asymmetric core
$\varepsilon, -$	0.514	0.547	$\varepsilon, -$	0.515	0.548
K_V, m^2	6.846×10^{-15}	4.999×10^{-15}	K_V, m^2	6.665×10^{-15}	4.903×10^{-15}
r_1, mm	26.65	26.65	r_2, mm	27.35	27.35
r_2, mm	27.35	27.35	r_3, mm	28.05	28.05
Parameters	Core ridge No. 3 Symmetric core	Asymmetric core	Parameters	Core ridge No. 4 Symmetric core	Asymmetric core
$\varepsilon, -$	0.520	0.553	$\varepsilon, -$	0.522	0.555
K_V, m^2	5.914×10^{-15}	4.345×10^{-15}	K_V, m^2	5.721×10^{-15}	4.201×10^{-15}
r_3, mm	28.05	28.05	r_4, mm	28.75	28.75
r_4, mm	28.75	28.75	r_5, mm	29.45	29.45
Parameters	Core ridge No. 5 Symmetric core	Asymmetric core	Parameters	Core ridge No. 6 Symmetric core	Asymmetric core
$\varepsilon, -$	0.529	0.552	$\varepsilon, -$	0.521	0.553
K_V, m^2	6.053×10^{-15}	4.449×10^{-15}	K_V, m^2	5.847×10^{-15}	4.356×10^{-15}
r_5, mm	29.45	29.45	r_6, mm	30.15	30.15
r_6, mm	30.15	30.15	r_7, mm	30.85	30.85
Parameters	Core ridge No. 7 Symmetric core	Asymmetric core	Parameters	Core ridge No. 8 Symmetric core	Asymmetric core
$\varepsilon, -$	0.522	0.553	$\varepsilon, -$	0.524	0.551
K_V, m^2	5.630×10^{-15}	4.348×10^{-15}	K_V, m^2	5.415×10^{-15}	4.632×10^{-15}
r_7, mm	30.85	30.85	r_8, mm	31.55	31.55
r_8, mm	31.55	31.55	r_9, mm	32.25	32.25
Parameters	Core ridge No. 9 Symmetric core	Asymmetric core	Parameters	Core ridge No. 10 Symmetric core	Asymmetric core
$\varepsilon, -$	0.533	0.554	$\varepsilon, -$	0.537	0.539
K_V, m^2	4.343×10^{-15}	4.317×10^{-15}	K_V, m^2	5.022×10^{-15}	6.044×10^{-15}
r_9, mm	32.25	32.25	r_{10}, mm	32.94	32.94
r_{10}, mm	32.94	32.94	r_{11}, mm	33.64	33.64
Parameters	Core ridge No. 11 Symmetric core	Asymmetric core			
$\varepsilon, -$	0.539	0.532			
K_V, m^2	4.821×10^{-15}	7.201×10^{-15}			
r_{11}, mm	33.64	33.64			
r_{12}, mm	34.35	34.35			

$$K_V = 2\varepsilon^{-12.98} \times 10^{-18}$$
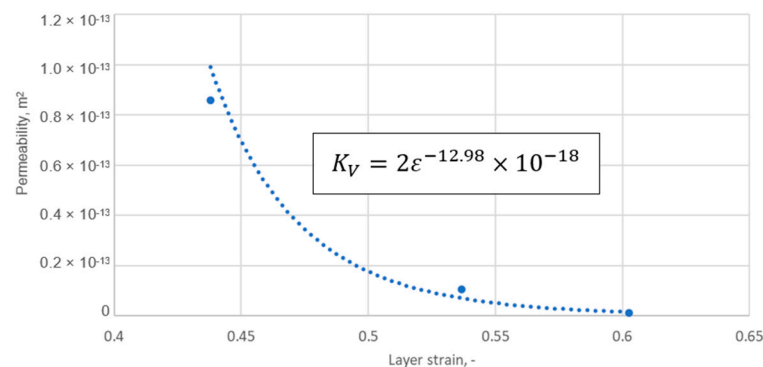
Figure 14. Permeability of the graphite layer as a function of layer strain.
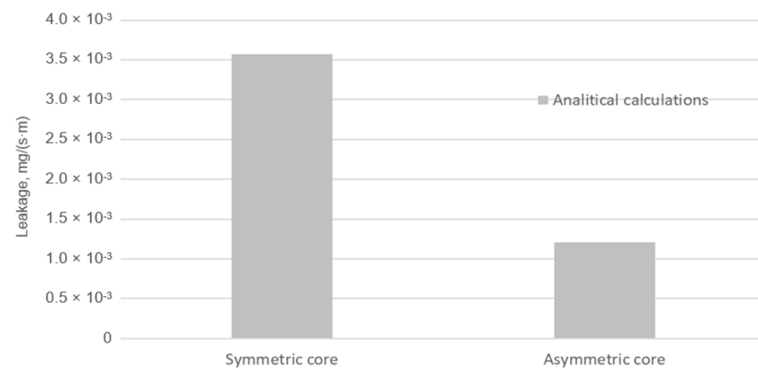
Figure 15. Leakage from the symmetrical and asymmetrical core gasket.

3.3. Results of Experimental Measurements

Figure 16 illustrates the leakage values measured experimentally at successive joint-tensioning steps.
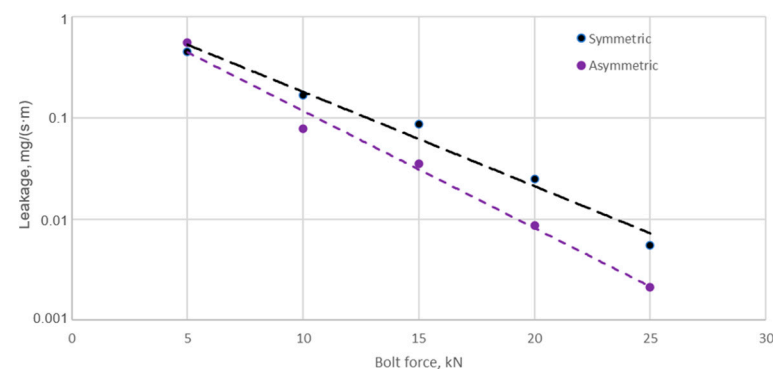

Figure 16. Leakage from the symmetrical and asymmetrical core gasket as a function of single bolt tension.

From the data shown in Figure 16, it can be seen that increasing the bolt tension of the joint leads to a progressively faster increase in leakage from the gasket with the asymmetric core compared to the gasket with the symmetric core. At a single bolt tension of 25 kN, the leakage from the symmetric core gasket is 5.48×10^{-3} mg/(s·m), while the leakage from the asymmetric core gasket is 2.12×10^{-3} mg/(s·m). This represents more than a 60% increase in the leakage of the gasket with the asymmetric core compared to the gasket with the symmetric core. Figure 17 summarises the leakage values measured experimentally against those obtained analytically (at a maximum bolt tension of 25 kN).
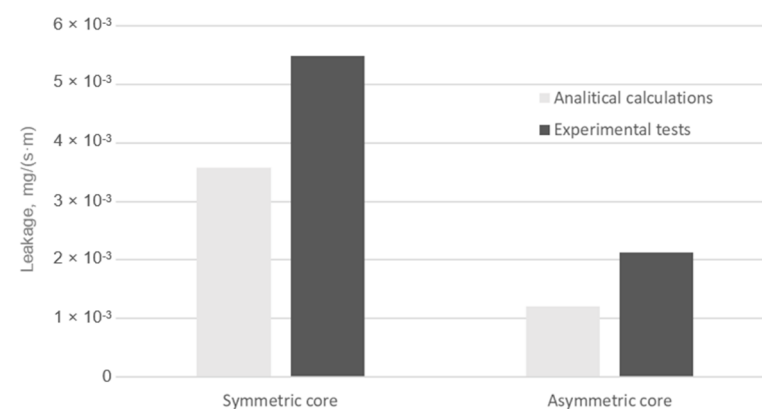

Figure 17. Leakage from the symmetrical and asymmetrical core gasket according to experimental tests and analytical calculations.

The percentage error between the mean value of the leakage measured experimentally and that obtained from analytical calculations is 34% and 43% for the symmetric core gasket and the asymmetric core gasket, respectively. The error between the measured and analytically calculated leakage is relatively large. This is a direct result of the measurement uncertainty of the detector used on the test stand, which can be as high as 30%. These differences may indicate a further need to expand the analytical model. On the other hand, both analytical calculations and measurements showed a higher sealing capacity for a gasket with an asymmetric core compared to a gasket with a symmetric core.

4. Discussion

4.1. Explanation of the Leakage Mechanism

The circumferential notch on the outer edge of the gasket core positively increased the strain in the graphite layer at the individual core ridges and resulted in a more uniform strain distribution of this layer along the width of the gasket. At the maximum tension force of a single bolt (i.e., 25 kN), the average strain value on ridges 1 to 9 is approximately 0.551. Only on the last two ridges (10 and 11) was there a slight decrease in strain to an average value of 0.535. In the case of a gasket with a symmetric core, the strain distribution of the graphite layer on the individual ridges is uneven. The smallest strain value (i.e., 0.514) occurs on the side of the inner gasket diameter and gradually increases towards the outer diameter, reaching a maximum strain value of 0.538. Only at the last two ridges does the strain of the graphite layer in the symmetric core approach values that are nearly identical to those occurring over the entire width range of the gasket with an asymmetric core. The increase in the strain of the graphite layer results in greater compaction of the pores in its internal structure and a more effective filling of the irregularities of the sealed metal surfaces, resulting in a reduction in leakage.

In general, the sealing mechanism at the interface of two surfaces separated by a sealing material should be considered in terms of two leakage components: the leakage component at the interface of the connected surfaces and the leakage component through the sealing material itself. In this case, the leakage model can be seen as a combination of two porous layers (in the form of rings) with different permeabilities and thicknesses. Consequently, the total leakage can be described by the following general form:

$$Q = Q\prime f(K_1) + Q''f(K_2) \tag{8}$$

The phenomenon of total leakage is also illustrated in Figure 18.
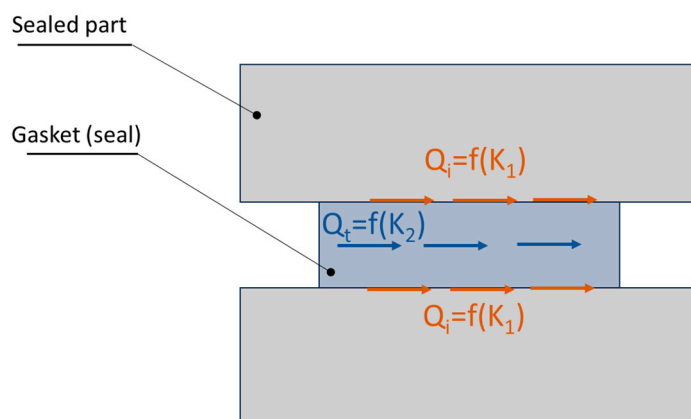

Figure 18. Potential leakage paths in the area of contact between two surfaces separated by sealing material.

The leakage component related to the permeability at interface K_1 depends mainly on the surface roughness. The second component K_2 depends mainly on the porosity of the sealing material. In both cases, the modelling of the leakage is reduced to the determination of the permeability of the porous layer K. The permeability K_1 can be specified by means of a fractal description of the surface roughness profile at the interface, as presented in [56,57]. The result of this approach is the determination of the permeability in the following form:

$$K_1 = \frac{\pi D_f \lambda_{max}^4}{128\tau\left(4 - D_f\right)S} \tag{9}$$

The main parameter of this model is the maximum pore diameter that forms between the contact of a flat surface and a rough surface and is related to the maximum peak of the roughness profile:

$$\lambda_{max} = \frac{S_{max,p} + \xi l_{max,p}}{P_{max,p} + 2\xi + l_{max,p}} \tag{10}$$

This diameter can be determined by measuring the roughness profile and identifying the constants G and D, which define the circumference and area of the maximum peak of the roughness profile.

Another parameter is capillary tortuosity, calculated from the following relationship:

$$\tau = \frac{1}{2}\left[1 + \frac{1}{2}\sqrt{1-\epsilon} + \sqrt{1-\epsilon}\frac{\sqrt{\left(\frac{1}{\sqrt{1-\epsilon}} - 1\right)^2 + \frac{1}{4}}}{1 - \sqrt{1-\epsilon}}\right] \tag{11}$$

Meanwhile, ϵ denotes the porosity of the bed, expressed in the following relationship:

$$\epsilon = \frac{V_{t,p1} + V_{t,p2}}{L_x L_y h} \tag{12}$$

where $V_{t,p1}$ and $V_{t,p2}$ denote the pore volume above and below the mean line of the roughness profile (the reference plane), respectively; $L_x L_y h$ indicates the product denoting the unit volume of the porous layer at the interface.

Another parameter that significantly affects the tightness is the fractal dimension of the capillary tortuosity, which is calculated from the following relationship:

$$D_f = 2 - \frac{\ln\epsilon}{\ln(\lambda_{min}/\lambda_{max})} \tag{13}$$

In the above model, the height of the porous layer can be calculated from the degree of penetration of the smooth layer into the rough one, using the fundamental laws of contact mechanics. Based on these laws, three basic deformation regimes are distinguished: elastic, elastoplastic, and plastic [56].

The permeability through the material can, in turn, be described using the model proposed in the following [58]:

$$K_2 = \frac{\pi D_f \left(\frac{\lambda_{max}}{2}\right)^{D_f}\left(\frac{\lambda_{max}}{2}^{3-D_f+D_t} - \frac{\lambda_{min}}{2}^{3-D_f+D_t}\right)}{2^{4-D_t}\sqrt{A^{1+D_t}}\left(3 - D_f + D_t\right)} \tag{14}$$

where D_t and A denote the fractal dimension of capillary tortuosity and the cross-sectional area of the representative element, respectively, calculated from the following relationships:

$$D_t = \left(2 - D_f + 1\right) + \left(2 - D_f\right)\frac{\ln D_f - \ln\left(D_f - 1\right)}{\ln\epsilon} \quad (15)$$

$$A = \frac{\pi D_f \left(\frac{\lambda_{max}}{2}\right)^{D_f}\left(\frac{\lambda_{max}}{2}^{2-D_f} - \frac{\lambda_{min}}{2}^{2-D_f}\right)}{\epsilon\left(2 - D_f\right)} \quad (16)$$

The dominance of one component of the leakage over the other depends on the type of gasket used and, more specifically, on the material from which the gasket is made.

In the case of a metal gasket, where the porosity of the structure is several orders of magnitude lower compared to a softer gasket material (e.g., made of expanded graphite), the sealing mechanism associated with the component at the interface of the connected surfaces dominates. In the case of a highly porous gasket, the component related to the leakage mechanism through the material itself dominates. Even with a small strain, the soft material very effectively fills the irregularities of the rough metal surface, so the main leakage occurs through the porous material structure. The differences between these two sealing mechanisms are shown in Figures 19 and 20.
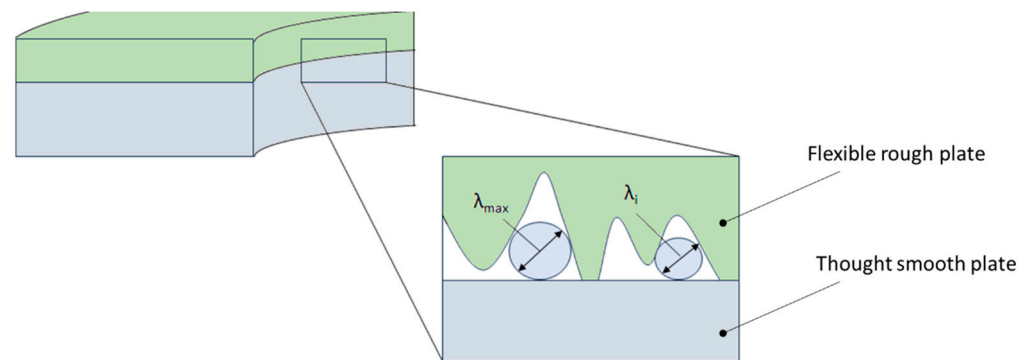

Figure 19. Potential leakage path at the metal–metal interface.
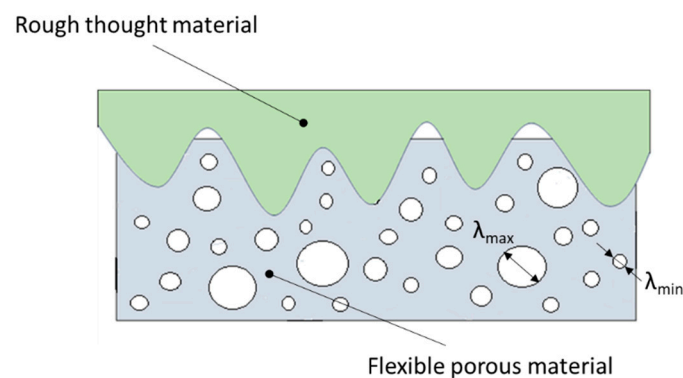

Figure 20. Potential leakage path at the metal–soft sealing material interface with a high porosity structure.

The multi-edge gasket presented in this paper combines both sealing mechanisms. Due to the high porosity of the graphite layer and the high deformability of the material, it effectively fills the irregularities of the metal surfaces, both at the interface of the joined flanges and at the interface with the metal core. Based on the sealing mechanism outlined above, it can be concluded that leakage through the graphite layer is the dominant component of leakage.

This can be evidenced through the research results reported in [59], in which the porosity and pore size distribution in the graphite layer were determined as a function of the contact pressure exerted on it—see Table 4.

Table 4. Selected properties of the graphite layer as a function of contact pressure [59].

Contact Pressure, MPa	Thickness, mm	Strain, -	Porosity, -	Max. Pore Diameter, mm	Min. Pore Diameter, mm
0	1.50	–	0.558	–	–
20	0.85	0.43	0.217	3.03×10^{-3}	0.54×10^{-3}
40	0.77	0.49	0.142	1.81×10^{-3}	0.20×10^{-3}
100	0.72	0.52	0.075	1.32×10^{-3}	0.09×10^{-3}

In Figure 21, the permeability values calculated using Equation (14) (based on data from Table 3) are compared with the experimentally determined permeability values. The values calculated by the model, compared to the measured ones, can be considered satisfactory. It can be seen that, in the strain range from 0.43 to 0.52, the permeability calculated through the model varies from 3.8×10^{-14} to 2.4×10^{-15}, while the experimentally determined permeability in the comparable strain range, i.e., from 0.44 to 0.53, varies from 8.6×10^{-14} to 1.2×10^{-15}.
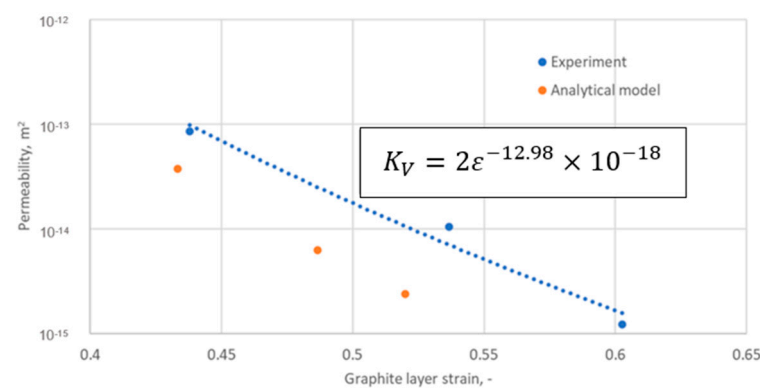

Figure 21. Permeability of the graphite layer as a function of graphite layer strain.

4.2. Effect of Gasket Width on Leakage

The outer notch in the core caused a significant increase in the average strain of the graphite layer. An increase in this strain (at the same tension force of a single bolt) can be achieved by reducing the gasket width. However, reducing the gasket width leads to increased leakage. The effect of decreasing the gasket width on leakage is well illustrated in the following equations:

$$Q = 2\pi KC \tag{17}$$

$$C = \frac{(1 - \varepsilon)}{\ln\beta} \tag{18}$$

where C denotes the coefficient linking the effect of strain and the relative width β of the ring on leakage.

The relative width, β, of the ring is expressed as the ratio of its outer radius to the inner radius. The effect of strain and the relative width, β, of the ring on the coefficient, C, is shown in Figure 22.
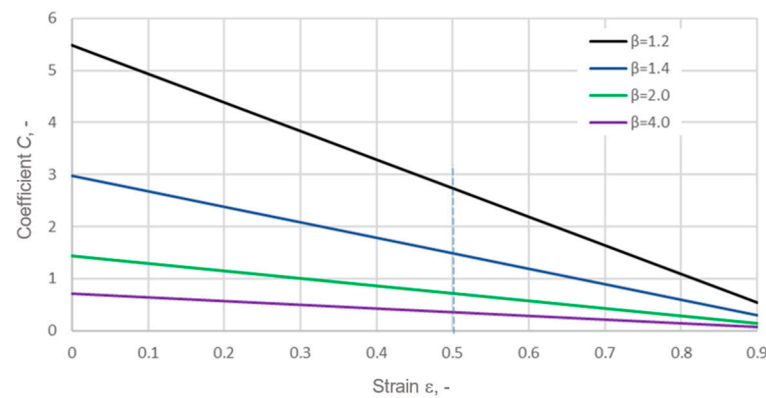
Figure 22. Effect of strain and the relative width of the ring on the coefficient, *C*.

It can be seen that, for a relatively small gasket width (i.e., for $\beta = 2$), a reduction in the gasket width leads to a multiple increase in the coefficient, C, which directly translates into an increase in leakage. Therefore, the design of a gasket with an asymmetric core allows the strain of the graphite layer to be increased without reducing the gasket width. Increasing the strain of the porous graphite layer results in greater compaction of the layer, which, in turn, reduces its permeability and leads to a higher degree of filling of the roughness profile of the surfaces to be sealed, quite like in the case of bonded surfaces [60,61].

5. Conclusions

Based on the performed calculations, the experimental studies, and the results obtained, the following conclusions can be drawn:

1. An increase in the strain of the graphite layer and its uniform distribution over the individual locking ridges can be achieved by notching the outer diameter of the metal core of the gasket. This leads to an extension of the strain and its uniformity across the width of the graphite layer. The average strain value of the graphite layer with the notched core (at the maximum joint tension force, i.e., 25 kN per bolt) rose by approximately 7% compared to the gasket with a symmetric core.
2. The increase in the average strain value of the graphite layer on the individual ridges in the gasket with the notched core resulted in an increase in tightness by approximately 60% compared to the gasket with the symmetric, non-notched core.
3. The greater the strain of the graphite layer, the better it fills the surface irregularities at the interface between the graphite layer and the metal flange surface, as well as at the interface between the graphite layer and the metal core of the gasket. Additionally, this results in greater compaction of the graphite material and a reduction in its porosity, which leads to a reduction in leakage.
4. Two distinctive sealing mechanisms can be distinguished in the considered design of a multi-edge gasket with expanded graphite inserts. The first occurs at the interface between the graphite layer and the metal surfaces, while the second takes place in the internal structure of the graphite layer. The level of tightness at the metal–graphite interface depends primarily on the height of the metal surface irregularities and the compressibility of the graphite. The level of tightness in the graphite layer depends mainly on its degree of compaction.
5. Due to the high elasticity of the graphite layer, there is an almost complete filling of the surface irregularities of the metal flanges at the interface with the metal core of the gasket. This means that leakage through the graphite material is the dominant component of leakage. This is evidenced by the results of analytical permeability calculations for the graphite layer, compared with the results obtained experimentally.

With a strain of the graphite layer in the range of 0.42 to 0.52, the calculated and experimentally measured permeability values fall within the same order of magnitude, i.e., from 1×10^{-14} to 1×10^{-15}, which, with such low values, makes the accuracy of the obtained results satisfactory.

6. At the maximum tension force (i.e., 25 kN per bolt), a friction coefficient at the graphite–metal interface in the range from 0.1 to 0.3 does not significantly affect the numerical calculations of the strain distribution in the graphite layer.

7. The paper considers only one type of asymmetry related to the circumferential notch on the outer diameter of the gasket. In order to address this limitation, the next step would be to investigate how changes in notch depth, position, or modification of the inner edge can affect the leakage behaviour.

8. In further phases of the research, it is planned to extend the test stand to allow leakage measurements at elevated temperatures.

9. It should also be noted as important to investigate larger gasket sizes. This is because, as the diameter increases, the width of the gasket also increases, which generally leads to greater variability in the contact pressure on the sealing surface.

References

1. Grzejda, R. FE-modelling of a contact layer between elements joined in preloaded bolted connections for the operational condition. *Adv. Sci. Technol. Res. J.* **2014**, *8*, 19–23. [CrossRef] [PubMed]

2. Grzejda, R. Modelling nonlinear preloaded multi-bolted systems on the operational state. *Eng. Trans.* **2016**, *64*, 525–531.

3. Jaszak, P. Prediction of the durability of a gasket operating in a bolted-flange-joint subjected to cyclic bending. *Eng. Fail. Anal.* **2021**, *120*, 105027. [CrossRef]

4. Jaszak, P.; Skrzypacz, J.; Borawski, A.; Grzejda, R. Methodology of leakage prediction in gasketed flange joints at pipeline deformations. *Materials* **2022**, *15*, 4354. [CrossRef] [PubMed]

5. Nozdrzykowski, K.; Chybowski, L.; Dorobczyński, L. Model-based estimation of the reaction forces in an elastic system supporting large-size crankshafts during measurements of their geometric quantities. *Measurement* **2020**, *155*, 107543. [CrossRef]

6. Chybowski, L.; Nozdrzykowski, K.; Grządziel, Z.; Dorobczyński, L. Evaluation of model-based control of reaction forces at the supports of large-size crankshafts. *Sensors* **2020**, *20*, 2654. [CrossRef]

7. Nozdrzykowski, K.; Grządziel, Z.; Dunaj, P. Determining geometrical deviations of crankshafts with limited detection possibilities due to support conditions. *Measurement* **2022**, *189*, 110430. [CrossRef]

8. Schneider, R.; Wuttke, U.; Berger, C. Fatigue analysis of threaded connections using the local strain approach. *Procedia Eng.* **2010**, *2*, 2357–2366. [CrossRef]

9. Nam, J.; Kim, D.; Kim, K.; Choi, S.; Hoon Oh, J. Unified fatigue life prediction of bolts with different sizes and lengths under various axial loading conditions. *Eng. Fail. Anal.* **2022**, *131*, 105841. [CrossRef]

10. Khan, N.B.; Abid, M.; Jameel, M.; Wajid, H.A. Joint strength of gasketed bolted pipe flange joint under combined internal pressure plus axial load with different (industrial and ASME) bolt-up strategy. *Proc. Inst. Mech. Eng. Part E J. Process Mech. Eng.* **2017**, *231*, 555–564. [CrossRef]

11. Romanik, G.; Jaszak, P.; Grzejda, R.; Zmarzły, P. Minimisation of friction resistance of elastomeric lip seals on rotating shafts. *Lubricants* **2024**, *12*, 103. [CrossRef]

12. Jaszak, P.; Oredsson, J.; Grzejda, R. Modelling of fluid permeability at the interface of the metal-to-metal sealing surface. *Materials* **2024**, *17*, 5194. [CrossRef] [PubMed]

13. Bouzid, H.; Beghoul, H. A New Proposed Method for the Design of Bolted Joints Based on Flexibility and Tightness. In Proceedings of the 10th International Conference on Pressure Vessel Technology, Vienna, Austria, 7–10 July 2003; pp. 293–301.

14. Abid, M.; Hussain, S. Relaxation behaviour of gasketed joints during assembly using finite element analysis. *Sādhanā* **2010**, *35*, 31–43. [CrossRef]

15. Aljuboury, M.; Rizvi, M.J.; Grove, S.; Cullen, R. A numerical investigation of the sealing performance and the strength of a raised face metallic bolted flange joint. *Int. J. Press. Vessel. Pip.* **2021**, *189*, 104255. [CrossRef]

16. Bouzid, A.; Chaaban, A.; Bazergui, A. The Influence of the Flange Rotation on the Leakage Performance of Bolted Flanged Joins. In Proceedings of the Canadian Society for Mechanical Engineering Forum, Montreal, QC, Canada, 27–29 June 1994; pp. 184–194.

17. Bouzid, A.; Derenne, M. Distribution of the Gasket Contact Stress in Bolted Flanged Connections. In Proceedings of the 1997 ASME/PVP Conference, Orlando, FL, USA, 27–31 July 1997; Volume 354, pp. 185–189.

18. Veiga, J.C.; da Silva, G.M.; Kavanagh, N. Factors That Influence the Sealing Behaviour of Spiral Wound Gasket. In Proceedings of the ASME 2013 Pressure Vessel and Piping Conference, Paris, France, 14–18 July 2013.

19. Attoui, H.; Bouzid, A.-H.; Waterland, J.A. Buckling and Lateral Pressures in Spiral Wound Gasket. In Proceedings of the ASME 2014 Pressure Vessels & Piping Conference, Anaheim, CA, USA, 20–24 July 2014.

20. Jenco, J.M.; Hunt, E.S. Generic issues effecting spiral wound gasket performance. *Int. J. Press. Vessel. Pip.* **2000**, *77*, 825–830. [CrossRef]

21. Roos, E.; Kockelmann, H.; Hahn, R. Gasket characteristics for the design of bolted flange connections of metal-to-metal contact type. *Int. J. Press. Vessel. Pip.* **2002**, *79*, 45–52. [CrossRef]

22. Abid, M.; Khan, K.A.; Chattha, J.A. Performance testing of a gasketed bolted flange pipe joint under combined pressure and thermal loading. *Exp. Tech.* **2011**, *35*, 35–37. [CrossRef]

23. Zhu, L.; Bouzid, A.-H.; Hong, J. Numerical and experimental study of elastic interaction in bolted flange joints. *J. Press. Vessel Technol.* **2017**, *139*, 021211. [CrossRef]

24. Gawande, S.H. Study on the effect of gasket thickness for bolted gearbox flange joint. *SN Appl. Sci.* **2019**, *1*, 32. [CrossRef]

25. He, L.; Lu, X.; Zhu, X.; Chen, Q. Influence of structural parameters of shape memory alloy corrugated gaskets on the contact pressure of bolted flange joints. *Adv. Mater. Sci. Eng.* **2021**, *2021*, 552569. [CrossRef]

26. Nechache, A.; Bouzid, A.-H. Creep analysis of bolted flange joints. *Int. J. Press. Vessel. Pip.* **2007**, *84*, 185–194. [CrossRef]

27. Murali Krishna, M.; Shunmugam, M.S.; Siva Prasad, N. A study on the sealing performance of bolted flange joints with gaskets using finite element analysis. *Int. J. Press. Vessel. Pip.* **2007**, *84*, 349–357. [CrossRef]

28. Bouzid, A.-H.; Galai, H. A new approach to model bolted flange joints with full face gaskets. *J. Press. Vessel Technol.* **2011**, *133*, 021203. [CrossRef]

29. Xu, W. Influence of flange structure parameters on contact pressure of the new-type wedge ring gasket. *Chem. Eng. Technol.* **2022**, *45*, 1312–1317. [CrossRef]

30. Rino Nelson, N.; Siva Prasad, N.; Sekhar, A.S. Structural integrity and sealing behaviour of bolted flange joint: A state of art review. *Int. J. Press. Vessel. Pip.* **2023**, *204*, 104975. [CrossRef]

31. Aljuboury, M.; Rizvi, M.J.; Grove, S.; Cullen, R. Bolted fibre-reinforced polymer flange joints for pipelines: A review of current practice and future challenges. *Proc. Inst. Mech. Eng. Part L J. Mater. Des. Appl.* **2019**, *233*, 1698–1717. [CrossRef]

32. Simonton, J.L.; Barry, L.K. Evolution of a more reliable gasket for HF alkylation units. *Seal. Technol.* **2006**, *2006*, 12–14. [CrossRef]

33. Veiga, J.C.; Cipolatti, C.F.; Kavanagh, N.; Castro, F.; Zandoná, V. Serrated Metal Graphite Faced Gaskets for Ring Joint Flanges. In Proceedings of the ASME 2012 Pressure Vessels and Piping Conference, Toronto, ON, Canada, 15–19 July 2012.

34. Jaszak, P. A new solution of the semi-metallic gasket increasing tightness level. *Open Eng.* **2019**, *9*, 329–337. [CrossRef]

35. Jaszak, P. The elastic serrated gasket of the flange bolted joints. *Int. J. Press. Vessel. Pip.* **2019**, *176*, 103954. [CrossRef]

36. Murugan, P.; Nagarajan, R.D.; Shetty, B.H.; Govindasamy, M.; Sundramoorthy, A.K. Recent trends in the applications of thermally expanded graphite for energy storage and sensors—A review. *Nanoscale Adv.* **2021**, *3*, 6294. [CrossRef]

37. *PN-EN 1514-6*; Flanges and their Joints, Dimensions of Gaskets for PN-Designated Flanges, Part 6: Covered Serrated Metal Gaskets for Use with Steel Flanges. Polish Committee for Standardization: Warsaw, Poland, 2005.

38. Mutz, A.; Schaaf, M. Comparison Between Different Calculation Methods for Determining Bolting up Moments. In Proceedings of the ASME 2016 Pressure Vessels and Piping Conference, Vancouver, BC, Canada, 17–21 July 2016.

39. Setiyorini, Y.; Pintowantoro, S.; Rahmat, A.; Ardian, F. The finite element analysis and the optimization design of shock absorber based on ANSYS. *AIP Conf. Proc.* **2021**, *2384*, 060001.

40. Ardian, F.; Setiyorini, Y.; Pintowantoro, S.; Hidayat, M.I.P.; Rahmat, A. Finite element analysis of new design artificial hip prosthesis. *AIP Conf. Proc.* **2021**, *2384*, 090003.

41. *PN-EN 1092-1*; Flanges and Their Joints, Circular Flanges for Pipes, Valves, Fittings and Accessories, PN Designated, Part 1: Steel Flanges. Polish Committee for Standardization: Warsaw, Poland, 2018.

42. Lošák, P.; Létal, T.; Nad', M.; Pernica, M. Tightness of flange joints: A case study. *IOP Conf. Ser. Mater. Sci. Eng.* **2020**, *776*, 012037. [CrossRef]

43. Wojnar, A.; Kozłowski, A. Mechanical model for assessment of the stiffness of bolted flanged joint. In *Progress in Steel, Composite and Aluminium Structures*; Giżejowski, M.A., Kozłowski, A., Ślęczka, L., Ziółko, J., Eds.; Taylor & Francis Group: London, UK, 2006; pp. 297–303.

44. Żyliński, B.; Buczkowski, R. Analysis of bolt joint using the finite element method. *Arch. Mech. Eng.* **2010**, *57*, 275–292. [CrossRef]

45. Rino Nelson, N.; Siva Prasad, N.; Sekhar, A.S. Stress distribution and performance of threaded bolts in gasketed flange joints. *Materialwiss. Werkstofftech.* **2021**, *52*, 982–990. [CrossRef]

46. Oredsson, J.; García, J.M.P. Multiphysics FEA Modelling of Gasketed Bolted Flange Joints. Available online: https://irp.cdn-website.com/724d6275/files/uploaded/Multiphysics_FEA_Modelling_of_Gasketed_Bolted_Flange_Joints-49128322.pdf (accessed on 25 May 2025).

47. Brown, W. *Determination of Pressure Boundary Joint Assembly Bolt Loads*, 2nd ed.; WRC Bulletin 538; Welding Research Council: Shaker Heights, OH, USA, 2014.

48. Estrada, H. Analysis of leakage in bolted-flanged joints using contact finite element analysis. *J. Mech. Eng. Autom.* **2015**, *5*, 135–142.

49. Aribas, U.N.; Atalay, M.; Omurtag, M.H. Warping included mixed finite elements for bending and stresses of functionally graded exact curved beams. *Mech. Adv. Mater. Struct.* **2023**, *31*, 5040–5056. [CrossRef]

50. Li, Y.; Lu, Y.; Wang, T.; Zhang, J. A new higher-order plate/shell element for dynamic analysis of flexible plate and shell with variable thickness. *Meccanica* **2023**, *58*, 1365–1383. [CrossRef]

51. *PN-EN 13555*; Flanges and Their Joints, Gasket Parameters and Test Procedures Relevant to the Design Rules for Gasketed Circular Flange Connections. Polish Committee for Standardization: Warsaw, Poland, 2021.

52. Létal, T. Estimating leak rates of circular gaskets under nonuniform contact pressures using EN 13555 test data. *Int. J. Press. Vessel. Pip.* **2022**, *200*, 104809. [CrossRef]

53. *DIN 28090-3*; Static Gaskets for Flange Connections, Gaskets Made from Sheets, Part 3: Chemical Resistance Test Procedures. German Institute for Standardization: Berlin, Germany, 2014.

54. Romanik, G.; Rogula, J.; Regucki, P. Investigation of the durability of gaskets in contact with bio- and aviation fuels. *Materials* **2022**, *15*, 6288. [CrossRef]

55. Demange, D.; Grivet, M.; Pialot, H.; Chambaudet, A. Indirect tritium determination by an original ^{3}He ingrowth method using a standard helium leak detector mass spectrometer. *Anal. Chem.* **2002**, *74*, 3183–3189. [CrossRef] [PubMed]

56. Zhang, Q.; Chen, X.; Huang, Y.; Chen, Y. Fractal modeling of fluidic leakage through metal sealing surfaces. *AIP Adv.* **2018**, *8*, 045310. [CrossRef]

57. Zheng, Q.; Xu, J.; Yang, B.; Yu, B. A fractal model for gaseous leak rates through contact surfaces under non-isothermal condition. *Appl. Therm. Eng.* **2013**, *52*, 54–61. [CrossRef]

58. Lei, G.; Liu, T.; Liao, Q.; He, X. Estimating permeability of porous media from 2D digital images. *J. Mar. Sci. Eng.* **2023**, *11*, 1614. [CrossRef]

59. Yurkov, A.L.; Malakho, A.P.; Ivanov, A.V.; Chernova, E.A.; Belogorlov, A.A.; Avdeev, V.V. Studying the porosity of graphite foil with different densities: Pore space model and gas permeability. *J. Mater. Sci.* **2022**, *57*, 21156–21171. [CrossRef]

60. Kubit, A.; Macek, W.; Zielecki, W.; Szawara, P.; Myśliwiec, P. Experimental study of the impact of notches and holes made in the front edge of adherends on the properties of static and fatigue strength of adhesive joints. *Int. J. Adhes. Adhes.* **2024**, *129*, 103596. [CrossRef]

61. Sługocka, M.; Grochała, D.; Kwiatkowski, K.; Grzejda, R.; Zmarzły, P. Study of the impact of surface topography on selected mechanical properties of adhesive joints. *Coatings* **2024**, *14*, 944. [CrossRef]